

Engineering ER-stress dependent non-conventional mRNA splicing

Tracking no: 24-01-2018-RA-eLife-35388R1

Impact statement: We characterized the evolutionary specialization of the unfolded protein response and engineered ER-stress dependent non-conventional mRNA splicing

Competing interests: No competing interests declared

Author contributions:

Weihan Li: Conceptualization; Data curation; Formal analysis; Validation; Investigation; Visualization; Methodology; Writing—original draft; Writing—review and editing Voytek Okreglak: Conceptualization; Data curation; Supervision; Methodology; Writing—review and editing Jirka Peschek: Supervision; Methodology; Writing—review and editing Phillip Kimmig: Conceptualization; Supervision; Methodology; Writing—review and editing Meghan Zubradt: Data curation; Formal analysis; Investigation; Methodology; Writing—review and editing Jonathan Weissman: Resources; Supervision; Funding acquisition; Writing—review and editing Peter Walter: Conceptualization; Resources; Supervision; Funding acquisition; Writing—review and editing

Funding:

Howard Hughes Medical Institute (HHMI): Jonathan S Weissman, Peter Walter; Human Frontier Science Program (HFSP): Jirka Peschek, Phillip Kimmig; National Science Foundation (NSF): Meghan Zubradt; Genentech Foundation: Meghan Zubradt; Center for RNA Systems Biology: Jonathan S Weissman; UCSF-Zaffaroni Fellowship: Weihan Li The funders had no role in study design, data collection and interpretation, or the decision to submit the work for publication.

Data Availability:

DMS-seq data has been deposited to Data Dryad. This dataset is available for review purpose through a temporary link: <http://datadryad.org/review?doi=doi:10.5061/dryad.s95f1>

Datasets Generated: Data from: Engineering ER-stress dependent non-conventional mRNA splicing: Li W, Okreglak V, Peschek J, Kimmig P, Zubradt M, Weissman J, Walter P, 2018, <http://datadryad.org/review?doi=doi:10.5061/dryad.s95f1>, This dataset is available for review purpose through a temporary link: <http://datadryad.org/review?doi=doi:10.5061/dryad.s95f1> Reporting Standards: N/A

Ethics:

Human Subjects: No Animal Subjects: No

Information for reviewers (full submissions):

eLife aims to publish work of the highest scientific standards and importance in all areas of the life and biomedical sciences, from the most basic and theoretical work through to translational, applied and clinical research. Articles must be methodologically and scientifically rigorous, ethically conducted, and objectively presented according to the appropriate community standards.

You will be asked for a general assessment and a summary of any major concerns (ideally in fewer than 500 words), as well as a list of any minor comments (optional). You will also have the opportunity to comment on the statistical rigour of the work (optional).

In your general assessment, please articulate what is exciting and whether the work represents a significant contribution. Please note our guidelines about requests for additional work:

1. We will only request new work, such as experiments, analyses, or data collection, if the new data are essential to support the major conclusions. The authors must be able to do any new work in a reasonable time frame (additional work should be conducted and written up within two months); otherwise, we will usually reject the manuscript.
2. Any requests for new work must fall within the scope of the current submission and the technical expertise of the authors.

Our goal is to make peer review constructive and collaborative: after the reviews have been submitted independently, there is an online discussion between the reviewers in which each reviewer will see the identity of the other reviewers.

1 **Engineering ER-stress dependent non-conventional mRNA splicing**

2

3 **Weihan Li^{1,*}, Voytek Okreglak^{1,3}, Jirka Peschek¹, Philipp Kimmig^{1,4}, Meghan**

4 **Zubradt², Jonathan Weissman², Peter Walter^{1,*}**

5

6 **¹Department of Biochemistry and Biophysics and Howard Hughes Medical**

7 **Institute, University of California San Francisco, CA 94143, USA**

8 **²Department of Cellular and Molecular Pharmacology and Howard Hughes**

9 **Medical Institute, University of California San Francisco, CA 94143, USA**

10 **³Current address: Calico Life Sciences LLC, South San Francisco, CA 94080, USA**

11 **⁴Current address: Institute of Biochemistry, ETH Zürich, Zürich, Switzerland**

12

13 ***: Corresponding authors**

14

15

16 **Abstract**

17 The endoplasmic reticulum (ER) protein folding capacity is balanced with the
18 protein folding burden to prevent accumulation of un- or misfolded proteins. The ER
19 membrane-resident kinase/RNase Ire1 maintains ER protein homeostasis through
20 two fundamentally distinct processes. First, Ire1 can initiate a transcriptional
21 response through a non-conventional mRNA splicing reaction to increase the ER
22 folding capacity. Second, Ire1 can decrease the ER folding burden through selective
23 mRNA decay. In *Saccharomyces cerevisiae* and *Schizosaccharomyces pombe*, the two
24 Ire1 functions have been evolutionarily separated. Here, we show that the
25 respective Ire1 orthologs have become specialized for their functional outputs by
26 divergence of their RNase specificities. In addition, RNA structural features separate
27 the splicing substrates from the decay substrates. Using these insights, we
28 engineered an *S. pombe* Ire1 cleavage substrate into a splicing substrate, which
29 confers *S. pombe* with both Ire1 functional outputs.

30

31 **Introduction**

32

33 In eukaryotes, the vast majority of secretory and transmembrane proteins
34 are folded in the endoplasmic reticulum (ER). The ER protein folding homeostasis is
35 maintained by a collective of signaling pathways, termed the unfolded protein
36 response (UPR) (Walter and Ron, 2011, Ron and Walter, 2007). The most
37 evolutionarily conserved branch of the UPR is mediated by the ER-transmembrane
38 kinase/endoribonuclease (RNase) Ire1. Direct binding of unfolded proteins to Ire1's
39 ER luminal domain triggers Ire1 to oligomerize and form foci (Gardner and Walter,
40 2011, Karagoz et al., 2017, Credle et al., 2005, Aragon, van Anken et al., 2009). In
41 turn, Ire1 oligomerization activates Ire1's cytosolic kinase/RNase domain
42 (Korenykh et al., 2009), which restores ER homeostasis through two functional
43 outputs. First, Ire1 initiates a process of non-conventional cytosolic splicing of *XBP1*
44 mRNA (in metazoans) or *HAC1* mRNA (in *S. cerevisiae*). Translation of the spliced
45 mRNA produces a transcription factor Xbp1 (Hac1 in *S. cerevisiae*), which drives a
46 large transcriptional program to adjust the ER's protein-folding capacity according
47 to the protein folding load in the ER lumen (Cox et al., 1993, Mori et al., 1993,
48 Yoshida et al., 2001, Calfon et al., 2002, Sidrauski et al., 1996). Second, Ire1 can
49 reduce the ER folding burden by cleaving a set of mRNAs encoding ER-target
50 proteins. The initial Ire1-mediated cleavage leads to mRNA degradation, in a
51 process termed regulated Ire1-dependent decay (RIDD) (Hollien and Weissman,
52 2006, Hollien et al., 2009, Kimmig, Diaz et al., 2012). The mechanism that

53 distinguishes the non-conventional mRNA splicing from RIDD has largely remained
54 unknown.

55

56 Interestingly, the two Ire1 modalities co-exist in metazoan cells (Hollien and
57 Weissman, 2006, Hollien et al., 2009, Moore and Hollien, 2015), yet are
58 evolutionarily separated in the two yeast species, *S. cerevisiae* and *S. pombe*. The
59 UPR in *S. cerevisiae* engages Ire1 exclusively in mRNA splicing, whereas in *S. pombe*
60 it engages Ire1 exclusively in RIDD. There is no detectable RIDD in *S. cerevisiae* and
61 no *HAC1/XBP1* ortholog in *S. pombe*, nor is there a corresponding transcriptional
62 program (Niwa et al., 2005, Kimmig, Diaz et al., 2012). It is intriguing to note that the
63 fundamental task of maintaining ER protein homeostasis can be achieved by two
64 radically different processes catalyzed by two distantly related Ire1 orthologs. The
65 two yeast species, *S. cerevisiae* and *S. pombe*, therefore provide a unique opportunity
66 to dissect the two Ire1 functional outputs, which has remained an unsolved
67 challenge in metazoans. Here, we set out to exploit this opportunity.

68

69 **Results**

70

71 ***S. pombe* and *S. cerevisiae* Ire1's cytosolic domains are functionally divergent**

72

73 Despite their common role as UPR effectors and conserved domain structure
74 (Fig. 1A), *S. pombe* and *S. cerevisiae* Ire1 orthologs share 29% sequence identity, and
75 sequence variation may confer Ire1's functional divergence. To explore this notion,
76 we swapped the homologous *IRE1* genes between the two yeast species by
77 expressing *S. cerevisiae* Ire1 in $\Delta ire1$ *S. pombe* cells and, *vice versa*, *S. pombe* Ire1 in
78 $\Delta ire1$ *S. cerevisiae* cells. To this end, we constructed strains in which we integrated
79 the foreign *IRE1* genes into the genomes of the other yeast such that their
80 expression was regulated by the host species-endogenous *IRE1* promoters and the
81 resulting mRNAs contained host species-endogenous 5' and 3' untranslated regions
82 (UTR). The *IRE1* genes contained sequences encoding FLAG-tags that we inserted
83 into an unstructured loop in their ER-luminal domains in a position known to
84 preserve Ire1 function (Rubio et al., 2011). In both yeasts, the foreign genes
85 expressed Ire1 at comparable levels (Fig. 1B & C, lanes 3). However, when grown on
86 plates containing tunicamycin, a drug that blocks N-linked glycosylation and induces
87 ER stress, the foreign Ire1s failed to support cell growth of either *S. pombe* and *S.*
88 *cerevisiae* cells (Fig. 1D & E, lanes 3), indicating that *S. pombe* and *S. cerevisiae* Ire1s
89 are not interchangeable.

90

91 There are two plausible, not mutually exclusive scenarios that could explain
92 the failure of cross-species complementation: i) the foreign Ire1 luminal domains
93 fail to sense ER stress, or ii) the foreign Ire1 cytosolic domains fail to recognize
94 species-appropriate RNA substrates. Since the Ire1 luminal domains have lower
95 sequence identity (21%) than the cytosolic kinase/RNase domains (45%), we first
96 swapped the Ire1 luminal domains, generating chimeras with foreign luminal
97 domains and host species-endogenous transmembrane/cytosolic domains. Both
98 chimeras supported growth on tunicamycin plates, suggesting that the divergent
99 Ire1 luminal domains share a conserved mechanism to sense ER stress and
100 transduce the signal across ER membrane (Fig. 1D & E, lanes 4). Next, we swapped
101 the Ire1 transmembrane/cytosolic domains. These Ire1 chimeras failed to restore
102 growth on tunicamycin plates of both *S. pombe* and *S. cerevisiae* cells (Fig. 1D & E,
103 lanes 5), indicating that the Ire1 transmembrane/cytosolic domains cause the Ire1
104 functional incompatibility when expressed in the opposing yeast. As a control, we
105 expressed FLAG-tagged host species-endogenous Ire1s into $\Delta ire1$ strains of both
106 yeasts. These strains phenocopied the wild type (WT) cells on tunicamycin plates
107 (Fig. 1D & E, lanes 6). We again confirmed by immunoblotting that all of the FLAG-
108 tagged Ire1 constructs were stably expressed at near-endogenous level in both
109 yeasts (Fig. 1B & C).

110

111 We next asked whether the Ire1 constructs would process the host species-
112 appropriate RNA substrates in *S. pombe* and *S. cerevisiae* cells. To this end, we
113 performed Northern blot and qPCR analyses to measure cleavage and subsequent

114 down-regulation of *GAS2* mRNA, which is a RIDD target in *S. pombe* cells (Kimmig,
115 Diaz et al., 2012). We performed the Northern blot in $\Delta ski2$ *S. pombe*, in which the
116 RNA 3' to 5' decay machinery is impaired so that the *GAS2* mRNA 5' cleavage
117 fragments can be detected in the gel. Of the different Ire1 variants, only the Ire1
118 chimera bearing the *S. pombe* cytosolic domain cleaved the *GAS2* mRNA (Fig. 1—
119 figure supplement 1A) and decreased the mRNA level (Fig. 1F), consistent with the
120 growth phenotype. In *S. pombe*, Ire1 also cleaves the *BIP1* mRNA within its 3'UTR,
121 producing a truncated mRNA with an increased half-life (Kimmig, Diaz et al., 2012).
122 To assess *BIP1* mRNA processing, we performed qPCR analysis using two pairs of
123 primers, one pair bracketing the Ire1 cleavage site and the other pair bracketing a
124 region upstream of it (Fig. 1G, schematic insert, *black* vs. *grey* arrows), reporting on
125 uncleaved only and both *BIP1* mRNA species (i.e. total *BIP1* mRNA), respectively. As
126 expected, upon tunicamycin-induced ER stress in WT cells uncleaved *BIP1* mRNA
127 levels decreased while total *BIP1* mRNA level increased (Fig. 1G, lanes 1, 2). As
128 shown in Figure 1G, Ire1 variants bearing the *S. pombe* cytosolic domain processed
129 *BIP1* mRNA, whereas Ire1 variants bearing the *S. cerevisiae* cytosolic domain did not.
130 This result is further validated by Northern blot analysis of *BIP1* mRNA (Fig. 1—
131 figure supplement 1B).

132

133 Correspondingly in *S. cerevisiae* cells, we examined *HAC1* mRNA splicing by
134 PCR across its splice junction. Consistent with the cell growth phenotype on
135 tunicamycin, the two Ire1 constructs bearing the *S. pombe* cytosolic domains did not
136 splice *HAC1* mRNA in *S. cerevisiae* cells (Fig. 1H, lanes 6, 10). By contrast, the Ire1

137 chimera bearing the *S. pombe* luminal domain and *S. cerevisiae* cytosolic domains
138 spliced *HAC1* mRNA (Fig. 1H, lane 8), albeit at reduced efficiency compared to WT *S.*
139 *cerevisiae* Ire1 (Fig. 1H, lane 2). We confirmed the activity of the various Ire1
140 constructs in *HAC1* mRNA splicing by monitoring UPR dynamics with a *HAC1* mRNA-
141 derived splicing reporter (Fig. 1—figure supplement 2A & B) previously described
142 (Aragon, van Anken et al., 2009, Zuleta et al., 2014). The reduced *HAC1* mRNA
143 splicing efficiency observed for Ire1 bearing the *S. pombe* luminal domain (Fig. 1H,
144 lane 8, and Fig. 1—figure supplement 2B, column 4) can be explained by the
145 observation that the *S. pombe* luminal domain mediates a lower degree of
146 oligomerization than its *S. cerevisiae* counterpart, as demonstrated by the reduced
147 ability of Ire1-mCherry fusion constructs to form foci visible by fluorescent
148 microscopy (Fig. 1—figure supplement 2C). Consistent with previous studies
149 (Aragon, van Anken et al., 2009), the insertion of the mCherry module into the Ire1
150 cytosolic linker, which connects Ire1 transmembrane domain and cytosolic
151 kinase/RNase domain, did not affect its ability to sustain cell growth (Fig. 1—figure
152 supplement 2D).

153

154 **Ire1 kinase/RNase domains have distinct RNase specificity**

155

156 To further confine the Ire1 region giving rise of the species differences in
157 outputs, we expressed an Ire1 chimera that, in addition to the *S. cerevisiae* luminal
158 domain, also included the *S. cerevisiae* transmembrane and cytosolic linker domains
159 fused to the *S. pombe* kinase/RNase domain. This chimeric Ire1 weakly rescued cell

160 growth and mildly restored the *HAC1* mRNA splicing upon ER stress (Fig. 2A lane 4,
161 & Fig. 2B lane 6), compared to the chimera containing *S. pombe* transmembrane and
162 cytosolic linker domains, although both constructs were expressed at similar
163 protein levels (Fig. 2C). This result indicates that the major difference lies in the
164 kinase/RNase domains, but that the transmembrane and cytosolic linker domains
165 can afford a marginal rescue, most likely by reintroducing cytosolic linker elements
166 that facilitate *HAC1* mRNA docking (van Anken et al., 2014).

167

168 To study the differences by which the Ire1 kinase/RNase domains select
169 their respective substrate mRNAs, we purified recombinant *S. cerevisiae* and *S.*
170 *pombe* kinase/RNase domains and performed *in vitro* RNA cleavage assays. The *S.*
171 *cerevisiae* Ire1 kinase/RNase efficiently cleaved a cognate 29-nucleotide RNA
172 hairpin derived from the 3' splice site of *S. cerevisiae HAC1* mRNA (Fig. 2D). By
173 contrast, under the same conditions the *S. pombe* Ire1 kinase/RNase cleaved the *S.*
174 *cerevisiae HAC1* mRNA-derived substrate ~60-fold slower (Fig. 2D). Reciprocally,
175 the *S. pombe* Ire1 kinase/RNase efficiently cleaved a cognate 32-nucleotide RNA
176 hairpin derived from the cleavage site in *S. pombe BIP1* mRNA and cognate RNA
177 hairpins derived from the RIDD cleavage sites in *S. pombe SPAC4G9.15* and *PLB1*,
178 whereas *S. cerevisiae* Ire1 kinase/RNase cleaved the *BIP1* mRNA-derived substrate
179 and the *S. pombe SPAC4G9.15* >500-fold slower and *PLB1* mRNA-derived hairpins
180 ~100-fold slower (Fig. 2E, F, G). These *in vitro* data validate and expand the
181 conclusions from the experiments conducted *in vivo*, suggesting that the different

182 Ire1 RNase specificities separate their functional outputs and that they are not
183 dependent on other cellular factors such as associated proteins or lipids.

184

185 **Ire1 kinase/RNase domains recognize distinct RNA sequence and structural**
186 **features**

187

188 Ire1 recognizes its substrates based on both RNA sequence and structural
189 features. The required RNA sequence motifs were characterized previously and
190 differ between species: for *S. cerevisiae* Ire1 a nucleotide sequence of CNG|CNGN or
191 CNG|ANGN ("|" indicates the Ire1 cleavage position) situated in a strictly conserved
192 7-membered loop is required (Gonzalez et al., 1999). By contrast, for *S. pombe* Ire1 a
193 three-nucleotide sequence of UG|C is required and no additional structural features
194 have yet been characterized (Kimmig, Diaz et al., 2012, Guydosh et al., 2017). To fill
195 this gap in our knowledge, we examined the RNA secondary structures *in vivo*. To
196 this end, we treated the *S. pombe* cells with dimethyl sulfate (DMS), which allows
197 detection of exposed (unpaired and not blocked by proteins) adenine/cytosine
198 residues (illustrated as green dots in Fig. 3A). RNA was extracted, reverse
199 transcribed and deep-sequenced. The DMS modifications stop reverse transcriptase
200 and generate truncated DNA fragments that we mapped through deep sequencing.
201 We then used identified unpaired bases to guide *in silico* RNA secondary structure
202 predictions (Rouskin et al., 2014). For example, near one of the *GAS2* mRNA
203 cleavage sites, five bases, labeled in green in Figure 3B, have high DMS modification
204 signals. In the RNA folding software mfold (Zuker, 2003), we provided the

205 constraint such that these five residues are unpaired and obtained the predicted
206 RNA secondary structure (Fig. 3C). In this structure, the *GAS2* mRNA forms a 9-
207 membered stem loop with the cleavage consensus sequence UG|C located near the
208 center of the loop. In similar analyses of 13 additional *S. pombe* Ire1 substrate mRNA
209 cleavage sites previously identified by both Kimmig, Diaz et al. and Guydosh et al.
210 (Guydosh et al., 2017, Kimmig, Diaz et al., 2012), we found in all of them cleavage
211 sites located near the center of loops in RNA stem-loop structures (Fig. 3—figure
212 supplement 1 A, B). By contrast to those found in *S. cerevisiae* *HAC1* mRNA, the
213 predicted loops were of variable sizes, with the smallest being a 3-membered loop
214 (e.g., the *SPAC4G9.15* mRNA cleavage site) and the largest being a 9-membered loop
215 (e.g., the *BIP1* mRNA cleavage site). We summarize that *S. pombe* Ire1 is tolerant to
216 loop size variation, while the *S. cerevisiae* Ire1 stringently recognizes 7-membered
217 stem loops. Thus, the *S. cerevisiae* and *S. pombe* Ire1 recognize distinct RNA
218 sequence and structural features (Fig. 3D).

219

220 A prediction of this model is that RNAs that combine *S. cerevisiae* and *S.*
221 *pombe* Ire1 motifs should be substrates to Ire1 from either species. To test this
222 prediction, we analyzed a substrate satisfying criteria for both species. Specifically,
223 we examined a substrate predicted to form a 7-membered stem loop with the
224 sequence CUG|CAGC, meeting the criteria of both the *S. cerevisiae* Ire1 motif
225 (CNG|CNGN) and the *S. pombe* Ire1 motif (UG|C). Indeed, both enzymes cleaved this
226 RNA *in vitro* with similar efficiency, in strong support of our model (Fig. 3E).

227

228 We further challenged the model *in vivo* by modifying the *S. pombe BIP1*
229 mRNA. First, we replaced the Ire1 cleavage site in the 3' UTR of *BIP1* mRNA with a
230 sequence derived from the *S. cerevisiae HAC1* mRNA 5' splice site. This modification
231 is predicted to change the endogenous 9-membered loop to a 7-membered one. The
232 new construct ('*BIP1-HAC1* hybrid mRNA') contained the sequence AG|C, which is
233 different from the *S. pombe* Ire1 sequence motif UG|C. In support of our model, *S.*
234 *pombe* Ire1 failed to cleave the *BIP1-HAC1* hybrid mRNA upon UPR induction (Fig.
235 3G, bar 3 & 4, Fig. 3—figure supplement 2A, B). Next, we mutated the non-cognate A
236 to a cognate U, such that the *S. pombe* Ire1 cleavage motif UG|C was restored. Indeed,
237 the single nucleotide change restored the *S. pombe* Ire1 cleavage (Fig. 3G, bar 5 & 6,
238 Fig. 3—figure supplement 2C). Taken together, we conclude that the Ire1 orthologs
239 in *S. cerevisiae* and *S. pombe* have divergent substrate preferences.

240

241 **Engineering non-conventional mRNA splicing in *S. pombe***

242

243 While these results revealed the differences between the *S. cerevisiae* and *S.*
244 *pombe* UPR at the step of Ire1 cleavage, it was not clear what determines the fates of
245 the RNA cleavage fragments, i.e. RNA ligation in *S. cerevisiae* and RNA degradation in
246 *S. pombe*. To address this question, we tested whether *S. pombe* cells contain
247 functional mRNA ligation machinery. To this end, we expressed the *S. cerevisiae*
248 *HAC1* mRNA-derived splicing reporter (Fig. 1—figure supplement 2A) in Δ *Ire1* *S.*
249 *pombe* cells, bearing genomic copies of various Ire1 constructs. A chimeric Ire1
250 bearing the *S. pombe* cytosolic domain failed to splice the reporter mRNA, in

251 agreement with our model (Fig. 4A, lane 5 & 6). Interestingly, both Ire1 constructs
252 bearing the *S. cerevisiae* cytosolic domains successfully spliced the reporter mRNA
253 (Fig. 4A, lanes 1-4). Thus, the *S. pombe* cells ligated the mRNA cleavage fragments as
254 long as the correct RNA substrates were provided. This result suggested that
255 features in the RNA substrates determine their fate post Ire1 cleavage.

256

257 Recently, we reported that in mammalian cells the *XBP1* mRNA actively
258 participates in the splicing reaction. In particular, a conformational RNA
259 rearrangement promotes *XBP1* mRNA intron ejection and exon ligation (Peschek,
260 Acosta-Alvear et al., 2015). We wondered if this mechanism could be the factor that
261 diverges the fates of the RNA cleavage fragments. To address this question, we
262 aimed to synthetically create the Ire1-dependent non-conventional mRNA splicing
263 reaction in *S. pombe* cells initiated by endogenous *S. pombe* Ire1. First, we identified
264 the analogous RNA conformational rearrangement in *S. cerevisiae* *HAC1* mRNA. To
265 obtain a *HAC1*-derived RNA splicing cassette optimized for *S. pombe* Ire1, we then
266 engineered the two Ire1-cleavage sites at the splice junctions to match the *S. pombe*
267 Ire1 UG|C motif and pruned the intron (originally 252 bp in *S. cerevisiae*) to the very
268 residues predicted to be critical for the mRNA conformational rearrangement (30
269 bp). Finally, we inserted the *S. pombe*-optimized mRNA splicing cassette into *S.*
270 *pombe* *BIP1* mRNA, replacing its endogenous Ire1 cleavage site (Fig. 4B, Fig. 4–figure
271 supplement 1). Indeed, we found that the *BIP1* mRNA containing the synthetic
272 splicing cassette was spliced in *S. pombe* upon induction of ER stress (Fig. 4C lane 2).
273 Sequencing of the lower band in Figure 4C (lane 2) verified the designed identity of

274 the splicing product (Fig. 4D). To show that insertion of the splicing cassette triggers
275 mRNA splicing independent of particular flanking elements, we inserted the splicing
276 cassette into the 3'UTR of another synthetic mRNA. In this case, we constructed a
277 synthetic mRNA containing the 5' UTR of tubulin (*NDA2*) mRNA, the open reading
278 frame of a *GAS2* mutant mRNA in which all of its RIDD cleavage sites were mutated,
279 and the 3' UTR of *NDA2* mRNA with the inserted splicing cassette (Fig. 4E). As for
280 the mRNA described above, this construct was efficiently spliced in *S. pombe* upon
281 ER stress (Fig. 4F). Thus, we conclude that the substrate RNA structure determines
282 the fate of the RNA cleavage fragments.

283

284

285 **Discussion**

286

287 "What I cannot create, I do not understand" (Richard Feynman). Inspired by
288 this quote, we engineered *S. pombe* cells to carry out a non-conventional mRNA
289 splicing reaction that does not occur in this species naturally. This feat was enabled
290 by a combination of a detailed mechanistic characterization of the differences in
291 Ire1-dependent mRNA processing between two yeast species reported in this paper
292 and by functional insights gleaned previously from a characterization of the
293 mammalian *XBP1* mRNA splicing mechanism (Peschek, Acosta-Alvear et al., 2015).
294 Two main conclusions emerged from this study. First, the evolutionary divergence
295 of Ire1's substrate specificity determines the set of mRNAs that are cleaved in either
296 species. Second, features in the mRNAs determine the distinct fates of the severed
297 mRNA fragments. *S. pombe* can be coopted to carry out the core non-conventional
298 mRNA splicing reaction with fidelity, as long as it is provided with a spliceable RNA
299 substrate that matches the specificity requirements of its endogenous Ire1. Albeit
300 not optimized in evolution for efficiency of the reaction, no other components (such
301 as the RNA ligase) need to be fundamentally specialized to mediate the core splicing
302 reaction.

303

304 Ire1 orthologs in *S. cerevisiae* and *S. pombe* recognize their cognate mRNA
305 substrates by discriminating both sequence and structural features. *S. pombe* Ire1
306 RNase specificity is more promiscuous, and has a broad substrate scope, in line with
307 its role to initiate degradation of many ER-bound mRNAs to reduce the ER's protein

308 folding burden. By contrast, *S. cerevisiae* Ire1's RNase specificity is very stringent
309 and specialized with *HAC1* mRNA being as its only substrate in the cell (Niwa et al.,
310 2005), in line with its role to produce a single transcription activator to drive UPR
311 target genes. In mammals, two paralogs of Ire1 are expressed in a tissue-specific
312 manner (Tsuru et al., 2013, Bertolotti et al., 2001). Ire1 α , which performs both *XBP1*
313 mRNA splicing and RIDD, recognizes a similar but longer RNA sequence motif,
314 CUG|CAG, displayed in stem-loop structures (Maurel et al., 2014). Interestingly, the
315 loop sizes that Ire1 α recognizes differ between the *XBP1* mRNA cleavage sites and
316 RIDD cleavage sites, with the two cleavage sites on *XBP1* mRNA to be conserved 7-
317 mer loops (Hooks and Griffiths-Jones, 2011), while the cleavage sites on RIDD
318 substrates vary in range from 9-mers to 5-mers (Fig. 4—figure supplement 2). This
319 suggests that mammalian Ire1 α may display two distinct modes of RNase activity—
320 a more stringent mode of RNase activity observed on 7-mer stem-loop RNAs (*XBP1*
321 mRNA and *BLOC1S* mRNA) and a more promiscuous mode of RNase activity on RNA
322 substrates with variable loop sizes. As shown here, these two modes have been
323 cleanly separated in evolution between *S. cerevisiae* and *S. pombe* Ire1. Hence it
324 seems plausible that mammalian Ire1 α may switch selectively into one or the other
325 state, perhaps in response to the timing of UPR activation or certain physiological
326 conditions, which could be reflected in particular oligomeric states, post-
327 translational modifications, or other effectors yet to be discovered.

328

329 Ire1 α is more efficient in *XBP1* mRNA splicing, while Ire1 β prefers to cleave
330 ribosomal RNA (Iwawaki et al., 2001, Nakamura et al., 2011, Imagawa et al., 2008).

331 Pairwise sequence alignment did not reveal an obvious similarity signatures that
332 would distinguish the Ire1 species performing for RIDD, i.e., *S. pombe* Ire1 and Ire1 β ,
333 from those engaged in mRNA splicing, i.e., *S. cerevisiae* Ire1 and Ire1 α (Fig. 4—figure
334 supplement 3A, B). On the substrate side, two Ire1 β cleavage sites both located on
335 rRNA, have been mapped to date. They share a common sequence of G|C at the
336 cleavage site. Previous studies indicated that differences in Ire1 α 's and Ire1 β 's
337 RNase domains lead to their functional distinction (Imagawa et al., 2008). We did
338 not observed cleavage of rRNA by *S. pombe* Ire1 (Fig. 1—figure supplement 1A, B);
339 mammalian Ire1 β 's activity to do so may therefore reflect a specialization that is not
340 generalizable to all Ire1 RNases that perform RIDD. Therefore, modulating Ire1's
341 RNase specificity to regulate its mode of action emerges as a general theme for
342 different species, as well as for different tissues within the same species.

343

344 In *S. cerevisiae* cells, apart from the *HAC1* mRNA, other mRNAs contain the *S.*
345 *cerevisiae* Ire1 cleavage motif, yet are not cleaved (Niwa et al., 2005). This is
346 explained by spatial coordination. *HAC1* mRNA is targeted to Ire1 upon stress,
347 utilizing a specific signal in the *HAC1* mRNA 3'UTR (Aragon, van Anken et al., 2009),
348 conferring exquisite specificity that renders *HAC1* mRNA the sole substrate of the
349 reaction. Although two other Ire1 substrate RNAs have been reported (Tam et al.,
350 2014), we have not been able to reproduce this result. By contrast to the dedicated
351 mRNA targeting in *S. cerevisiae*, *S. pombe* and mammalian cells target *XBP1* mRNA
352 and most RIDD substrates to the ER via the signal recognition particle (SRP)
353 pathway (Hollien and Weissman, 2006, Hollien et al., 2009, Yanagitani et al., 2009,

354 Yanagitani et al., 2011, Plumb et al., 2015). In this way, *S. pombe* and mammalian
355 Ire1 efficiently sample through substrate RNAs at ER periphery, which they cleave
356 more promiscuously. We presume that in our experimental set-up, the chimeric
357 *BIP1*-mRNA containing the splicing cassette would hijack the SRP-mediated
358 targeting route initiated by the BiP1 signal sequence, as we previously showed for
359 other RIDD substrate mRNAs (Kimmig, Diaz et al., 2012).

360

361 After Ire1 cleavage, RNA fragments are ligated or degraded, depending on the
362 substrate RNA structures. According to this notion, in mammalian cells where
363 splicing and RIDD co-exist, we predict that *XBP1* mRNA splicing and RIDD substrate
364 degradation are separated post Ire1 cleavage. The two cleavage sites on the *XBP1*
365 mRNA are coordinated by a zipper-like RNA structure, which enable the exons to be
366 held in juxtaposition and ligated by the cytosolic tRNA ligase (Peschek, Acosta-
367 Alvear et al., 2015, Sidrauski et al., 1996, Jurkin et al., 2014, Lu et al., 2014,
368 Kosmaczewski et al., 2014). By contrast, cleavage sites on the RIDD substrates lack
369 such coordination and the cleavage fragments are further degraded.

370

371 Our study revealed that Ire1's RNase specificity and its RNA substrate
372 structure separate Ire1's modes of action, opening the door to identify residues that
373 shape Ire1's RNase specificity. In this way, it should now become possible to design
374 metazoan Ire1s that favor mRNA splicing over RIDD, and *vice versa*, enabling us to
375 discriminate the biological significance of the two Ire1 functional outputs separately
376 in physiological and pathological contexts.

377 **Acknowledgement**

378

379 The *Dire1 S. pombe* strain was a generous gift from the Krogan lab (UCSF). We
380 thank Ignacio Zuleta, Benjamin Heineike and Alain Bonny for their help and
381 discussion on automated flow cytometry. We thank Wallace Marshall, Marc Shuman
382 and members of the Walter lab for their insightful discussions. This work was
383 supported by UCSF-Zaffaroni Fellowship (WL), the Human Frontier Science
384 Program (JP, PK), National Science Foundation grant 1144247 (MZ), the Genentech
385 Foundation (MZ) and CRSB (Center for RNA Systems Biology; grant P50 GM102706
386 to JSW). PW and JSW are Investigators of the Howard Hughes Medical Institute.

387

388 **Competing Financial Interests**

389

390 The authors declare no competing financial interests.

391

392 **Figure 1**
393 ***S. pombe* and *S. cerevisiae* Ire1 have functionally conserved stress sensing ER-**
394 **luminal domains and divergent cytosolic domains.** (A) Cartoon illustration of
395 luminal domain (LD), transmembrane/cytosolic linker domain (TMD+L) and
396 kinase/RNase domain (KR) for *S. pombe* (*Sp*) (*blue*) and *S. cerevisiae* (*Sc*) Ire1
397 (*orange*). (B, C) Expression levels of *S. cerevisiae* Ire1 (128 kD), *S. cerevisiae* luminal
398 *S. pombe* cytosolic Ire1 (126 kD), *S. pombe* luminal *S. cerevisiae* cytosolic Ire1 (125
399 kD) and *S. pombe* Ire1 (122 kD) in *S. pombe* (B) and *S. cerevisiae* cells (C). Extracts
400 were immunoblotted for 3xFLAG-Ire1. Ponceau stain (B) or Pgk1 (C) was used as
401 loading control. (D, E) Cell growth assay on tunicamycin (Tm) plates. Serial dilutions
402 of *S. pombe* (D) or *S. cerevisiae* (E) cells, which expressed the indicated Ire1
403 constructs, were spotted onto plates containing 0.05 µg/ml (B) or 0.1 µg/ml (C) of
404 Tm. Plates were photographed after incubation at 30° C for 4 days. (F, G) qPCR assay
405 for *S. pombe* *GAS2* (F) or *BIP1* (G) mRNA fold change upon 1 µg/ml Tm treatment for
406 1 h. Experiments were done in triplicates. In (G), uncleaved (*dark grey*) or total
407 (*light grey*) *BIP1* mRNA was detected using the corresponding PCR primers
408 illustrated as arrows in the schematic insert. The red dashed line indicates the Ire1
409 cleavage position on *BIP1* mRNA. (H) Detection of *S. cerevisiae* *HAC1* mRNA splicing
410 by RT-PCR across the splice junction. Cells were treated with or without 1 µg/ml of
411 Tm for 1 h.
412

413 **Figure 1—figure supplement 1**
414 **Ire1 chimeras with *S. pombe* cytosolic domain cleave *BIP1* and *GAS2* mRNA in *S.***
415 ***pombe*.** Northern blots of *S. pombe* *GAS2* (A) and *BIP1* (B) mRNA. Cells were treated
416 with 1 µg/ml of Tm for 1 h.
417

418 **Figure 1—figure supplement 2**

419 **Ire1 oligomeric state determines the *HAC1* mRNA splicing dynamics in *S.***

420 *cerevisiae* cells. (A) Illustration of the *HAC1* mRNA derived splicing reporter. The
421 splicing reporter contains a part of the *HAC1* mRNA 5' exon replaced by the green
422 fluorescent protein (GFP) coding sequence. In the unspliced reporter mRNA,
423 translation is inhibited by a translation block formed by the intron and 5'UTR
424 (indicated by the red arrow). Upon splicing, intron is removed and translation
425 begins. (B) Measuring the *HAC1* mRNA splicing dynamics in *S. cerevisiae* using
426 automated flow cytometry. After 1.5 h of incubation, either no Tm or 0.25 µg/ml, 0.5
427 µg/ml, 1 µg/ml, 2 µg/ml of Tm was added. Then, we monitored the splicing
428 dynamics for 10 h. The splicing dynamics under various conditions is plotted. *Green*
429 lines represent the strains of interest, which expressed indicated Ire1 variants, and
430 the *black* line represents WT control strain under the same condition. (C)
431 Examining Ire1 foci formation in *S. cerevisiae* cells via fluorescence microscopy with
432 or without 1 µg/ml Tm treatment for 20 min. (D) Growth assay on Tm plate for *S.*
433 *cerevisiae* cells expressing Ire1 constructs with or without mCherry inserted into the
434 cytosolic linker. The inserted mCherry does not affect Ire1's ability to alleviate ER
435 stress.

436

437 **Figure 2**

438 ***S. pombe* and *S. cerevisiae* Ire1 have distinct RNase specificity.** (A) Growth assay
439 for *S. cerevisiae* cells expressing indicated Ire1 constructs on Tm plates, as Figure 1E.
440 (B) Measuring *HAC1* mRNA splicing, as Figure 1H. (C) Comparing the expression
441 levels of the indicated 3xFLAG-tagged Ire1 chimeras using immunoblotting. Ponceau
442 stain was used as loading control. (D, E, F, G) *In vitro* RNA cleavage assays. 5'-
443 radiolabeled hairpin RNA substrates were incubated with 12.5 μ M *S. cerevisiae* or *S.*
444 *pombe* Ire1 kinase/RNase domains (KR) at 30° C for the indicated time. (D) Hairpin
445 RNA substrate derived from the 3' splice site of *S. cerevisiae HAC1* mRNA. The
446 calculated k_{obs} is $9.4 \pm 0.9 \times 10^{-4} s^{-1}$ for *S. cerevisiae* Ire1 KR and $0.15 \pm 0.01 \times 10^{-4} s^{-1}$
447 for *S. pombe* Ire1 KR. (E) Hairpin RNA substrate derived from the Ire1 cleavage site
448 on *S. pombe BIP1* mRNA. The calculated k_{obs} is $0.079 \pm 0.0006 \times 10^{-4} s^{-1}$ for *S.*
449 *cerevisiae* Ire1 KR and $37.3 \pm 4.4 \times 10^{-4} s^{-1}$ for *S. pombe* Ire1 KR. (F) Hairpin RNA
450 substrate derived from the Ire1 cleavage site on *S. pombe SPAC4G9.15* mRNA,
451 encoding a gene of unknown function. The calculated k_{obs} was below our detection
452 limit for *S. cerevisiae* Ire1 KR and $15.6 \pm 2.2 \times 10^{-4} s^{-1}$ for *S. pombe* Ire1 KR. (G)
453 Hairpin RNA substrate derived from the Ire1 cleavage site on *S. pombe PLB1* mRNA.
454 The calculated k_{obs} is $0.2 \pm 0.003 \times 10^{-4} s^{-1}$ for *S. cerevisiae* Ire1 KR and $19.0 \pm 2.5 \times$
455 $10^{-4} s^{-1}$ for *S. pombe* Ire1 KR.

456

457 **Figure 3**
458 ***S. pombe* and *S. cerevisiae* Ire1 recognize distinct RNA sequence and structural**
459 **features.** (A) Illustration of RNA structural mapping by DMS modifications.
460 Dimethyl sulfate (DMS) allows detection of unpaired adenine and cytosine RNA
461 bases (*green* dots). (B) The normalized DMS modification signals near the Ire1
462 cleavage site on *S. pombe* *GAS2* mRNA (cleavage site is indicated by the *red* dashed
463 line). The positions with high DMS modification signals are labeled in *green* and the
464 previously identified *S. pombe* Ire1 UG|C motif is labeled in *red*. (C) *In silico* RNA
465 secondary structure prediction of the Ire1 cleavage site on *GAS2* mRNA. Structure
466 prediction was constrained by forcing the positions with high DMS modification
467 signals (*green*) to be unpaired. (D) RNA sequence and structural motifs recognized
468 by the *S. cerevisiae* and *S. pombe* Ire1. (E) *In vitro* cleavage assay using an RNA
469 hairpin derived from human *XBP1* mRNA 3' splice site, which is predicted to be a
470 shared substrate for *S. cerevisiae* and *S. pombe* Ire1 KR. The calculated k_{obs} is $16.7 \pm$
471 $2.3 \times 10^{-4} \text{ s}^{-1}$ for *S. cerevisiae* Ire1 KR and $38.9 \pm 4.0 \times 10^{-4} \text{ s}^{-1}$ for *S. pombe* Ire1 KR.
472 (F) Illustrations of the *S. pombe* *BIP1* mRNA variants and (G) their uncleaved (*dark*
473 *grey*) or total (*light grey*) mRNA fold change upon ER stress in *S. pombe* cells.
474 Experiments were done in triplicates.
475

476 **Figure 3—figure supplement 1**

477 ***S. pombe* Ire1 cleaves at UG|C positioned near the center of loops in RNA stem-**

478 **loop structures.** (A) A list of all 14 *S. pombe* Ire1 mRNA cleavage sites, which were

479 independently identified by both Kimmig, Diaz et al. and Guydosh et al. (Guydosh et

480 al., 2017, Kimmig, Diaz et al., 2012). The UG|C motifs are labeled in *red*. The

481 positions with high DMS modification signals are labeled in *green*. (B) Predicted

482 RNA secondary structures of *S. pombe* Ire1 cleavage sites. DMS modification signals

483 were used to guide the secondary structure prediction of *S. pombe* Ire1 mRNA

484 cleavage sites. The *red* dashed lines indicate the Ire1 cleavage sites.

485

486 **Figure 3—figure supplement 2**

487 **Ire1 cleavage sites on *BIP1* mRNA variants.** Sequence and predicted RNA
488 secondary structures of Ire1 cleavage sites on (A) *S. pombe BIP1* mRNA, (B) *BIP1-*
489 *HAC1* hybrid mRNA and (C) *BIP1-HAC1* hybrid mRNA with an A to U mutation. The
490 part included in the dashed box is derived from *S. cerevisiae HAC1* mRNA 5' splice
491 site.

492

493 **Figure 4**
494 **Engineering the Ire1-mediated non-conventional mRNA splicing in *S. pombe***
495 **cells.** (A) Measuring the non-conventional mRNA splicing in *S. pombe* cells, which
496 were transformed with the *S. cerevisiae HAC1* mRNA splicing reporter and the
497 indicated Ire1 constructs. Cells were treated with 1 µg/ml Tm for 1 h. (B)
498 Illustration of the engineered *S. pombe BIP1* mRNA splicing variant. (C) Measuring
499 the nonconventional mRNA splicing of the engineered *S. pombe BIP1* mRNA splicing
500 variant. Experimental conditions are the same as those for Figure 4A. (D)
501 Sequencing reads of the spliced *BIP1* mRNA. The schematic illustrations (E) and the
502 splicing assays (F) of the synthetic splicing substrates in *S. pombe*. Cells were treated
503 with 1 µg/ml Tm for 1 h.

504

505 **Figure 4—figure supplement 1**

506 **The splicing cassette in the engineered *S. pombe* *BIP1* mRNA splicing variant.**

507 The part included in the dashed box is the inserted synthetic splicing cassette. The

508 *red* dashed lines indicate the Ire1 cleavage sites. The *S. pombe* Ire1 UG|C motifs are

509 labeled in red.

510

511 **Figure 4—figure supplement 2**

512 **The Ire1 α cleavage sites on *XBP1* mRNA and a RIDD targets.** Red dashed lines

513 mark the cleavage sites and the red letters indicate the previously identified

514 sequence motif.

515

516 **Figure 4—figure supplement 3**
517 **The sequence alignment of the kinase/RNase domains of Ire1 α , Ire1 β , the *S.***
518 ***cerevisiae* Ire1 and the *S. pombe* Ire1. (A) The sequence alignment and colored**
519 **with BoxShade Server. (B) The sequence identities between the indicated pairs of**
520 **Ire1 constructs.**
521

522 **Materials and Methods:**

523

524 **Strains, plasmids and growth conditions**

525 Standard *S. cerevisiae* and *S. pombe* genome editing and growth conditions were
526 used (Moreno et al., 1991, Guthrie and Fink, 2002). Strains used in this study are
527 listed in the Table 1. Specifically, all Ire1 constructs have a 3x FLAG-tag in their
528 luminal domains replacing an unstructured region (255-274 in *S. pombe* and 267-
529 286 in *S. pombe*). *S. cerevisiae* Ire1 domain boundaries were previously described
530 (Rubio et al., 2011), *S. pombe* Ire1 domains were determined by sequence alignment
531 with *S. cerevisiae* Ire1. Specifically, the luminal domain is 1-526 for *S. cerevisiae* and
532 1-507 for *S. pombe*. The transmembrane/cytosolic linker is 527-672 for *S. cerevisiae*
533 and 508-651 for *S. pombe*. Kinase/RNase is 673-1115 for *S. cerevisiae* and 652-1073
534 for *S. pombe*. Ire1 constructs were integrated into the *HO* locus in *S. cerevisiae*
535 (backbone plasmid: HO-Poly-KanMX4-HO) and *Leu* locus in *S. pombe* (backbone
536 plasmid: pJK148). *S. pombe* *BIP1* variants were integrated at the *BIP1* locus through
537 homologous recombination and uracil selection. The mCherry-tagged Ire1
538 constructs and the splicing reporter were previously described (Aragon, van Anken
539 et al., 2009).

540

541 **Growth assay**

542 Serial dilutions of *S. cerevisiae* or *S. pombe* cells were spotted onto YPD plates with
543 0.1 µg/ml tunicamycin (for *S. cerevisiae*) or YE5S plates with 0.05 µg/ml

544 tunicamycin (for *S. pombe*). Plates were photographed after incubating at 30° C for 4
545 days.

546

547 **Immunoblotting**

548 For both *S. cerevisiae* and *S. pombe* cells, total protein was isolated from yeast
549 cultures growing at exponential phase by vortexing with glass beads in 8 M urea, 50
550 mM HEPES, pH 7.4, and 1% sodium dodecylsulfate (SDS). Samples were boiled and
551 then centrifuged at 16,000 x g for 10 min. A sample containing 20 µg total protein
552 was separated using electrophoresis and then transferred to nitrocellulose. The
553 3xFLAG-tagged Ire1 was probed with monoclonal anti-FLAG antibody (Sigma
554 F3165).

555

556 **qPCR assays**

557 Total RNA was purified from yeast cultures using phenol extraction (Kohrer and
558 Domdey, 1991). RNA samples were resuspended in RNase-free water and quantified
559 by spectrophotometry. cDNA was synthesized by reverse transcription using
560 random hexamer DNA primers (Thermo Fisher Scientific), SuperScript II Reverse
561 Transcriptase (Thermo Fisher Scientific) and 1 µg total RNA as described previously
562 (Kimmig, Diaz et al., 2012). 1% of the cDNAs was employed for qPCR reactions using
563 SYBR green qPCR kit (Bio-Rad). qPCR was performed in triplicates using CFX96
564 Touch Real-Time PCR Detection System (Bio-rad). qPCR primers are listed in Table
565 2. mRNA levels were normalized to *NDA2* mRNA in *S. pombe*.

566

567 ***In vivo* mRNA splicing assay**

568 cDNA was synthesized the same way as described in the qPCR section. Then we
569 used Phusion High-Fidelity PCR Kit (NEB) and performed PCR with cDNA and a set
570 of primers across the splice junction. For *HAC1* mRNA, the forward primer was
571 ATGGAATGACTGATTTTGAAC TAACTAGTAATT CG. The reverse primer was
572 TCATGAAGTGATGAAGAAATCATTCAATTCAAATG. The PCR was performed for 26
573 cycles with annealing temperature of 51.5° C and extension time of 30 s. For the *S.*
574 *pombe BIP1* mRNA containing the splicing cassette, the forward primer was
575 GAATCGTGACTCTATAGCCATTAACA. The reverse primer was
576 CAATTATTGTCAGTTCCACAAAGC. The PCR was performed for 36 cycles with
577 annealing temperature of 63.4° C and extension time of 15 s. For *S. cerevisiae HAC1*
578 mRNA derived splicing reporter expressed in *S. pombe* cells, the forward primer was
579 GAACTACAAGACACGTGCTGAAG. The reverse primer was
580 GATGAAGAAATCATTCAATTCAAATG. The PCR was performed for 60 cycles with
581 annealing temperature of 63.2° C and extension time of 20 s. For the synthetic
582 splicing substrate in *S. pombe*, the forward primer was
583 CTCATTTAGATTAGCAATTCAAATG. The reverse primer was
584 GATTAGATCAACAATTCAAATGATC. The PCR was performed for 40 cycles with
585 annealing temperature of 59.7° C and extension time of 20 s.

586

587 **Recombinant protein purification**

588 *S. cerevisiae* Ire1 kinase/RNase was purified as previously described (Korenykh et
589 al., 2009). Details of the *S. pombe* Ire1 kinase/RNase purification will be described in

590 a separate paper. Briefly, *S. pombe* Ire1 kinase/RNase was N-terminally fused with
591 Glutathione S-transferase (GST) tag through a linker containing Human Rhinovirus
592 (HRV) 3C protease cleavage site, and was regulated by T7 promoter. This *S. pombe*
593 Ire1 kinase/RNase expression cassette was transformed into *E. coli* cells. 16 h after
594 transformation, we mixed and collected all the colonies on the transformation plates
595 by scraping them off from the agar plate into 50 ml of LB medium. After 3-hour
596 incubation at 37° C, the sample was diluted to 12 l of LB medium and further
597 incubated at 37° C until optical density reached 1. Protein expression was induced
598 by adding 0.5 mM IPTG. Then, the culture was incubated at 25° C for 4 h before we
599 pelleted the cells by centrifugation. Cells were resuspended in GST binding buffer
600 (50 mM Tris/HCl pH 7.5, 500 mM NaCl, 2 mM Mg(OAc)₂, 2 mM DTT, 10% Glycerol)
601 and homogenized using high-pressure homogenizer (EmulsiFlex, Avestin). The cell
602 lysate was applied to GST-affinity column and eluted with GST elution buffer (50
603 mM Tris/HCl pH 7.5, 200 mM NaCl, 2 mM Mg(OAc)₂, 2 mM DTT, 10% Glycerol, 10
604 mM glutathione). The column elution was treated with GST-tagged HRV 3C protease
605 (PreScission Protease, GE Health). At the same time, the sample was dialyzed to
606 remove glutathione in the elution buffer. Next, the sample was further purified
607 through negative chromatography by passing through a GST-affinity column (to
608 remove free GST and residue GST-fused Ire1 kinase/RNase) and an anion exchange
609 column (to remove contaminating nucleic acids). Finally, the sample was subject to
610 gel filtration, concentrated to about 14 μM in storage buffer (50 mM Tris/HCl pH
611 7.5, 200 mM NaCl, 2 mM Mg(OAc)₂, 2 mM TCEP, 10% Glycerol), and flash frozen in

612 liquid nitrogen. The final purity, as well as purity at intermediate steps, was
613 assessed by SDS-PAGE using Coomassie blue staining.

614

615 ***In vitro* RNA cleavage assays**

616 Short RNA oligos were purchased from Dharmacon, Inc. RNA oligos were gel
617 extracted, acetone precipitated and resuspended in RNase-free water. Then, oligos
618 were 5' end radio-labeled with γ -[³²P]-ATP (Perkin Elmer) using T4 polynucleotide
619 kinase (NEB) and cleaned using ssDNA/RNA Clean and Concentrator kit (Zymo
620 Research D7010). To fold the RNA oligos, we heated the RNA oligos to 90° C for 3
621 min and slowly cooled them down at a rate of 1° C per minute until the temperature
622 reached 10° C. In the Ire1 cleavage assays, the reaction samples contained 12.5 μ M
623 of *S. cerevisiae* or *S. pombe* Ire1 kinase/RNase. The cleavage reaction was performed
624 at 30° C in reaction buffer (50 mM Tris/HCl pH 7.5, 200 mM NaCl, 2 mM Mg(OAc)₂, 2
625 mM TCEP, 10% Glycerol). At each time point, an aliquot of 0.75 μ l was transferred to
626 5 μ l STOP buffer (10 M urea, 0.1% SDS, 1 mM EDTA, 0.05% xylene cyanol, 0.05%
627 bromophenol blue). RNAs were separated using denaturing 15% urea-PAGE gels
628 (run at 100 V for 90 min). Gels were imaged with a Phosphorimager (Typhoon FLA
629 9500, GE Health) and the band intensities were quantified using imageJ. The cleaved
630 portion was calculated as the cleaved band intensity divided by the sum of the
631 cleaved band and uncleaved band intensities. The k_{obs} were obtained by fitting the
632 data to first-order (“one-phase”) decay equation using Prism. For the cleavage
633 reactions that less than 10% of the substrates were cleaved, because the substrate
634 concentration was approximately constant, the cleavage dynamics was fitted to a

635 linear equation to obtain k_{obs} . The sequence of hairpin RNA substrate derived from
636 Ire1 cleavage site on *S. pombe BIP1* mRNA is
637 CGCGAGAUAACUGGUGCUUUGUUAUCUCGCG.

638 The sequence of hairpin RNA substrate derived from Ire1 cleavage site on *S. pombe*
639 *SPAC4G9.15* mRNA is CCACCACCGAGUAUGCUACUCGGUGGUGG.

640 The sequence of hairpin RNA substrate derived from *S. cerevisiae HAC1* mRNA 3'
641 splice site is GCGCGGACUGUCCGAAGCGCAGUCCGCGC

642 The sequence of hairpin RNA substrate derived from *XBP1* mRNA 3' splice site is
643 UGCACCUCUGCAGCAGGUGCA.

644

645 **Automated flow cytometry**

646 Measuring *S. cerevisiae* UPR dynamics using automated flow cytometry was
647 previously described in detail (Zuleta et al.). Briefly, we co-cultured two *S. cerevisiae*
648 strains, a strain of interest and a control strain. The control strain contained a
649 constitutively expressed mCherry reporter. The signal from the control strain was
650 computationally separate based on its high mCherry level. In an 11.5-hour time
651 course at 30° C, a data point was taken every 20 min. 1.5 h after inoculation, DMSO
652 (as control) or 0.25 µg/ml, 0.5 µg/ml, 1 µg/ml, 2 µg/ml of Tm were added. Splicing
653 dynamics were monitored for another 10 h. The GFP signal was normalized to the
654 signal at time zero.

655

656 **Probing *in vivo* mRNA structure in *S. pombe* cells**

657 A culture of 15 ml *S. pombe* cells, which were exponentially growing at 30° C, was
658 treated with 400 µl of DMS for 3.5 min. DMS was then quenched by adding 30 ml of
659 solution containing 30% β-mercaptoethanol and 25% isoamyl alcohol. Then, cells
660 were pelleted by centrifugation at 4° C, and washed with 15 ml 30% β-
661 mercaptoethanol. Total RNA was extracted using phenol extraction. Poly(A)+
662 mRNAs were isolated using poly(A)+ Dynabeads (Invitrogen). The sequencing
663 library was generated and sequenced, and the DMS modifications were computed as
664 previously described (Rouskin et al.).

665

666 **mRNA secondary structure prediction**

667 Near the Ire1 cleavage sites, we first identified the most highly reactive base and set
668 its DMS modification signal as 1. Then, the DMS modification signal raw data for
669 other bases was normalized proportionally. Finally, we put a 38-base-pair RNA
670 sequence (19 base pair upstream and downstream from the Ire1 cleavage site) into
671 the RNA secondary structure prediction program mfold (Zuker, 2003). Bases with
672 normalized DMS modification signals >0.2 were forced to be single stranded to
673 constrain the RNA folding prediction.

674

675

676 **Reference**

677

- 678 ARAGON, T., VAN ANKEN, E., PINCUS, D., SERAFIMOVA, I. M., KORENNYKH, A. V.,
679 RUBIO, C. A. & WALTER, P. 2009. Messenger RNA targeting to endoplasmic
680 reticulum stress signalling sites. *Nature*, 457, 736-40.
681
- 682 BERTOLOTTI, A., WANG, X., NOVOA, I., JUNGREIS, R., SCHLESSINGER, K., CHO, J. H.,
683 WEST, A. B. & RON, D. 2001. Increased sensitivity to dextran sodium sulfate
684 colitis in IRE1beta-deficient mice. *J Clin Invest*, 107, 585-93.
685
- 686 CALFON, M., ZENG, H., URANO, F., TILL, J. H., HUBBARD, S. R., HARDING, H. P.,
687 CLARK, S. G. & RON, D. 2002. IRE1 couples endoplasmic reticulum load to
688 secretory capacity by processing the XBP-1 mRNA. *Nature*, 415, 92-6.
689
- 690 COX, J. S., SHAMU, C. E. & WALTER, P. 1993. Transcriptional induction of genes
691 encoding endoplasmic reticulum resident proteins requires a
692 transmembrane protein kinase. *Cell*, 73, 1197-206.
693
- 694 CREDLE, J. J., FINER-MOORE, J. S., PAPA, F. R., STROUD, R. M. & WALTER, P. 2005. On
695 the mechanism of sensing unfolded protein in the endoplasmic reticulum.
696 *Proc Natl Acad Sci U S A*, 102, 18773-84.
697
- 698 GARDNER, B. M. & WALTER, P. 2011. Unfolded proteins are Ire1-activating ligands
699 that directly induce the unfolded protein response. *Science*, 333, 1891-4.
700
- 701 GONZALEZ, T. N., SIDRAUSKI, C., DORFLER, S. & WALTER, P. 1999. Mechanism of
702 non-spliceosomal mRNA splicing in the unfolded protein response pathway.
703 *EMBO J*, 18, 3119-32.
704
- 705 GUTHRIE, C. & FINK, G. R. 2002. *Guide to yeast genetics and molecular and cell*
706 *biology*, Amsterdam ; Boston ; London, Academic Press.
707
- 708 GUYDOSH, N. R., KIMMIG, P., WALTER, P. & GREEN, R. 2017. Regulated Ire1-
709 dependent mRNA decay requires no-go mRNA degradation to maintain
710 endoplasmic reticulum homeostasis in *S. pombe*. *Elife*, 6, e29216
711
- 712 HOLLIEN, J., LIN, J. H., LI, H., STEVENS, N., WALTER, P. & WEISSMAN, J. S. 2009.
713 Regulated Ire1-dependent decay of messenger RNAs in mammalian cells. *J*
714 *Cell Biol*, 186, 323-31.
715
- 716 HOLLIEN, J. & WEISSMAN, J. S. 2006. Decay of endoplasmic reticulum-localized
717 mRNAs during the unfolded protein response. *Science*, 313, 104-7.
718

719 HOOKS, K. B. & GRIFFITHS-JONES, S. 2011. Conserved RNA structures in the non-
720 canonical Hac1/Xbp1 intron. *RNA Biol*, 8, 552-6.
721

722 IMAGAWA, Y., HOSODA, A., SASAKA, S., TSURU, A. & KOHNO, K. 2008. RNase
723 domains determine the functional difference between IRE1alpha and
724 IRE1beta. *FEBS Lett*, 582, 656-60.
725

726 IWAWAKI, T., HOSODA, A., OKUDA, T., KAMIGORI, Y., NOMURA-FURUWATARI, C.,
727 KIMATA, Y., TSURU, A. & KOHNO, K. 2001. Translational control by the ER
728 transmembrane kinase/ribonuclease IRE1 under ER stress. *Nat Cell Biol*, 3,
729 158-64.
730

731 JURKIN, J., HENKEL, T., NIELSEN, A. F., MINNICH, M., POPOW, J., KAUFMANN, T.,
732 HEINDL, K., HOFFMANN, T., BUSSLINGER, M. & MARTINEZ, J. 2014. The
733 mammalian tRNA ligase complex mediates splicing of XBP1 mRNA and
734 controls antibody secretion in plasma cells. *EMBO J*, 33, 2922-36.
735

736 KARAGOZ, G. E., ACOSTA-ALVEAR, D., NGUYEN, H. T., LEE, C. P., CHU, F. & WALTER,
737 P. 2017. An unfolded protein-induced conformational switch activates
738 mammalian IRE1. *Elife*, 6, e30700
739

740 KIMMIG, P., DIAZ, M., ZHENG, J., WILLIAMS, C. C., LANG, A., ARAGON, T., LI, H. &
741 WALTER, P. 2012. The unfolded protein response in fission yeast modulates
742 stability of select mRNAs to maintain protein homeostasis. *Elife*, 1, e00048.
743

744 KOHRER, K. & DOMDEY, H. 1991. Preparation of high molecular weight RNA.
745 *Methods Enzymol*, 194, 398-405.
746

747 KORENNYKH, A. V., EGEA, P. F., KOROSTELEV, A. A., FINER-MOORE, J., ZHANG, C.,
748 SHOKAT, K. M., STROUD, R. M. & WALTER, P. 2009. The unfolded protein
749 response signals through high-order assembly of Ire1. *Nature*, 457, 687-93.
750

751 KOSMACZEWSKI, S. G., EDWARDS, T. J., HAN, S. M., ECKWAHL, M. J., MEYER, B. I.,
752 PEACH, S., HESSELBERTH, J. R., WOLIN, S. L. & HAMMARLUND, M. 2014. The
753 RtcB RNA ligase is an essential component of the metazoan unfolded protein
754 response. *EMBO Rep*, 15, 1278-85.
755

756 LU, Y., LIANG, F. X. & WANG, X. 2014. A synthetic biology approach identifies the
757 mammalian UPR RNA ligase RtcB. *Mol Cell*, 55, 758-70.
758

759 MAUREL, M., CHEVET, E., TAVERNIER, J. & GERLO, S. 2014. Getting RIDD of RNA:
760 IRE1 in cell fate regulation. *Trends Biochem Sci*, 39, 245-54.
761

762 MOORE, K. & HOLLIEN, J. 2015. Ire1-mediated decay in mammalian cells relies on
763 mRNA sequence, structure, and translational status. *Mol Biol Cell*, 26, 2873-
764 84.

765
766 MORENO, S., KLAR, A. & NURSE, P. 1991. Molecular genetic analysis of fission yeast
767 *Schizosaccharomyces pombe*. *Methods Enzymol*, 194, 795-823.
768
769 MORI, K., MA, W., GETHING, M. J. & SAMBROOK, J. 1993. A transmembrane protein
770 with a *cdc2+*/CDC28-related kinase activity is required for signaling from the
771 ER to the nucleus. *Cell*, 74, 743-56.
772
773 NAKAMURA, D., TSURU, A., IKEGAMI, K., IMAGAWA, Y., FUJIMOTO, N. & KOHNO, K.
774 2011. Mammalian ER stress sensor IRE1beta specifically down-regulates the
775 synthesis of secretory pathway proteins. *FEBS Lett*, 585, 133-8.
776
777 NIWA, M., PATIL, C. K., DERISI, J. & WALTER, P. 2005. Genome-scale approaches for
778 discovering novel nonconventional splicing substrates of the Ire1 nuclease.
779 *Genome Biol*, 6, R3.
780
781 PESCHEK, J., ACOSTA-ALVEAR, D., MENDEZ, A. S. & WALTER, P. 2015. A
782 conformational RNA zipper promotes intron ejection during non-
783 conventional XBP1 mRNA splicing. *EMBO Rep*, 16, 1688-98.
784
785 PLUMB, R., ZHANG, Z. R., APPATHURAI, S. & MARIAPPAN, M. 2015. A functional link
786 between the co-translational protein translocation pathway and the UPR.
787 *Elife*, 4, e07426.
788
789 RON, D. & WALTER, P. 2007. Signal integration in the endoplasmic reticulum
790 unfolded protein response. *Nat Rev Mol Cell Biol*, 8, 519-29.
791
792 ROUSKIN, S., ZUBRADT, M., WASHIETL, S., KELLIS, M. & WEISSMAN, J. S. 2014.
793 Genome-wide probing of RNA structure reveals active unfolding of mRNA
794 structures in vivo. *Nature*, 505, 701-5.
795
796 RUBIO, C., PINCUS, D., KORENNYKH, A., SCHUCK, S., EL-SAMAD, H. & WALTER, P.
797 2011. Homeostatic adaptation to endoplasmic reticulum stress depends on
798 Ire1 kinase activity. *J Cell Biol*, 193, 171-84.
799
800 SIDRAUSKI, C., COX, J. S. & WALTER, P. 1996. tRNA ligase is required for regulated
801 mRNA splicing in the unfolded protein response. *Cell*, 87, 405-13.
802
803 TAM, A. B., KOONG, A. C. & NIWA, M. 2014. Ire1 has distinct catalytic mechanisms for
804 XBP1/HAC1 splicing and RIDD. *Cell Rep*, 9, 850-8.
805
806 TSURU, A., FUJIMOTO, N., TAKAHASHI, S., SAITO, M., NAKAMURA, D., IWANO, M.,
807 IWAWAKI, T., KADOKURA, H., RON, D. & KOHNO, K. 2013. Negative feedback
808 by IRE1beta optimizes mucin production in goblet cells. *Proc Natl Acad Sci U*
809 *SA*, 110, 2864-9.
810

811 VAN ANKEN, E., PINCUS, D., COYLE, S., ARAGON, T., OSMAN, C., LARI, F., GOMEZ
812 PUERTA, S., KORENNYKH, A. V. & WALTER, P. 2014. Specificity in
813 endoplasmic reticulum-stress signaling in yeast entails a step-wise
814 engagement of HAC1 mRNA to clusters of the stress sensor Ire1. *Elife*, 3,
815 e05031.
816
817 WALTER, P. & RON, D. 2011. The unfolded protein response: from stress pathway to
818 homeostatic regulation. *Science*, 334, 1081-6.
819
820 YANAGITANI, K., IMAGAWA, Y., IWAWAKI, T., HOSODA, A., SAITO, M., KIMATA, Y. &
821 KOHNO, K. 2009. Cotranslational targeting of XBP1 protein to the membrane
822 promotes cytoplasmic splicing of its own mRNA. *Mol Cell*, 34, 191-200.
823
824 YANAGITANI, K., KIMATA, Y., KADOKURA, H. & KOHNO, K. 2011. Translational
825 pausing ensures membrane targeting and cytoplasmic splicing of XBP1u
826 mRNA. *Science*, 331, 586-9.
827
828 YOSHIDA, H., MATSUI, T., YAMAMOTO, A., OKADA, T. & MORI, K. 2001. XBP1 mRNA
829 is induced by ATF6 and spliced by IRE1 in response to ER stress to produce a
830 highly active transcription factor. *Cell*, 107, 881-91.
831
832 ZUKER, M. 2003. Mfold web server for nucleic acid folding and hybridization
833 prediction. *Nucleic Acids Res*, 31, 3406-15.
834
835 ZULETA, I. A., ARANDA-DIAZ, A., LI, H. & EL-SAMAD, H. 2014. Dynamic
836 characterization of growth and gene expression using high-throughput
837 automated flow cytometry. *Nat Methods*, 11, 443-8.
838
839
840

841 **Table 1:**
842 Yeast strains used in this study. All strains are derived from WL001 and WL002. All
843 Ire1 constructs listed below are 3x FLAG-tagged within their luminal domains.
844

strain	species	description
yWL001	<i>Sc</i>	WT, mat A, <i>leu2-3,112 TRP1 can1-100 ura3-1 ADE2 his3-11,15</i>
yWL002	<i>Sc</i>	<i>ire1Δ::NAT^R</i>
yWL003	<i>Sc</i>	<i>ire1Δ::NAT^R, HO::Sp IRE1</i>
yWL004	<i>Sc</i>	<i>ire1Δ::NAT^R, HO::SpLumScCyto IRE1</i>
yWL005	<i>Sc</i>	<i>ire1Δ::NAT^R, HO::ScLumSpCyto IRE1</i>
yWL006	<i>Sc</i>	<i>ire1Δ::NAT^R, HO::Sc IRE1</i>
yWL007	<i>Sc</i>	<i>ire1Δ::NAT^R, HO::ScLum/transmembrane/linkerSpKR IRE1</i>
yWL008	<i>Sc</i>	WT, <i>leu2::5'hac1-gfp-3'hac1</i>
yWL009	<i>Sc</i>	<i>ire1Δ::NAT^R, leu2::5'hac1-gfp-3'hac1</i>
yWL010	<i>Sc</i>	<i>ire1Δ::NAT^R, leu2::5'hac1-gfp-3'hac1, HO::Sp IRE1</i>
yWL011	<i>Sc</i>	<i>ire1Δ::NAT^R, leu2::5'hac1-gfp-3'hac1, HO:: SpLumScCyto IRE1</i>
yWL012	<i>Sc</i>	<i>ire1Δ::NAT^R, leu2::5'hac1-gfp-3'hac1, HO:: ScLumSpCyto IRE1</i>
yWL013	<i>Sc</i>	<i>ire1Δ::NAT^R, leu2::5'hac1-gfp-3'hac1, HO::Sc IRE1</i>
yWL014	<i>Sc</i>	<i>leu2::5'hac1-gfp-3'hac1, his3::pTdh3-mCherry</i>
yWL015	<i>Sp</i>	WT, mat h ⁺ , <i>ade6-M210, ura4-D18, leu1-32</i>
yWL016	<i>Sp</i>	<i>ire1Δ::KAN^R</i>
yWL017	<i>Sp</i>	<i>ire1Δ::KAN^R, leu1::Sp IRE1</i>
yWL018	<i>Sp</i>	<i>ire1Δ::KAN^R, leu1::SpLumScCyto IRE1</i>
yWL019	<i>Sp</i>	<i>ire1Δ::KAN^R, leu1::ScLumSpCyto IRE1</i>
yWL020	<i>Sp</i>	<i>ire1Δ::KAN^R, leu1::Sc IRE1</i>
yWL021	<i>Sp</i>	<i>ire1Δ::KAN^R, leu1::SpLumScCyto IRE1, ura4::5'hac1-gfp-3'hac1</i>
yWL022	<i>Sp</i>	<i>ire1Δ::KAN^R, leu1::ScLumSpCyto IRE1, ura4::5'hac1-gfp-3'hac1</i>
yWL023	<i>Sp</i>	<i>ire1Δ::KAN^R, leu1::Sc IRE1, ura4::5'hac1-gfp-3'hac1</i>
yWL024	<i>Sp</i>	<i>bip1::bip1-hac1</i> hybrid
yWL025	<i>Sp</i>	<i>bip1::bip1-hac1</i> hybrid A->U
yWL026	<i>Sp</i>	<i>bip1::bip1</i> splicing variant
yWL027	<i>Sp</i>	<i>ura4::synthetic</i> splicing substrate

845
846

847 **Table 1:**
848 qPCR primers used in this study.
849

qPCR primers description	sequence
uncleaved <i>Sp BiP1</i> mRNA forward primer	GAATCGTGACTCTATAGCCATTAACA
uncleaved <i>Sp BiP1</i> mRNA reverse primer	CAATTATTGTCAGTCCACAAAGC
total <i>Sp BiP1</i> mRNA forward primer	TGGTAAGGTTGATCCCGAAG
total <i>Sp BiP1</i> mRNA reverse primer	CATCGAGTTTTTGACGCTGA
<i>Sp GAS2</i> mRNA forward primer	GTTGTCAACAATGCCTCGAA
<i>Sp GAS2</i> mRNA reverse primer	CGGTCTCAGAGTTGGTGTCA
<i>Sp NDA2</i> mRNA forward primer	TCCATGAATCCAACAGCGTA
<i>Sp NDA2</i> mRNA reverse primer	CTAGTAACGGCAGCCTGGAC

850
851

Fig 1 Li et al.

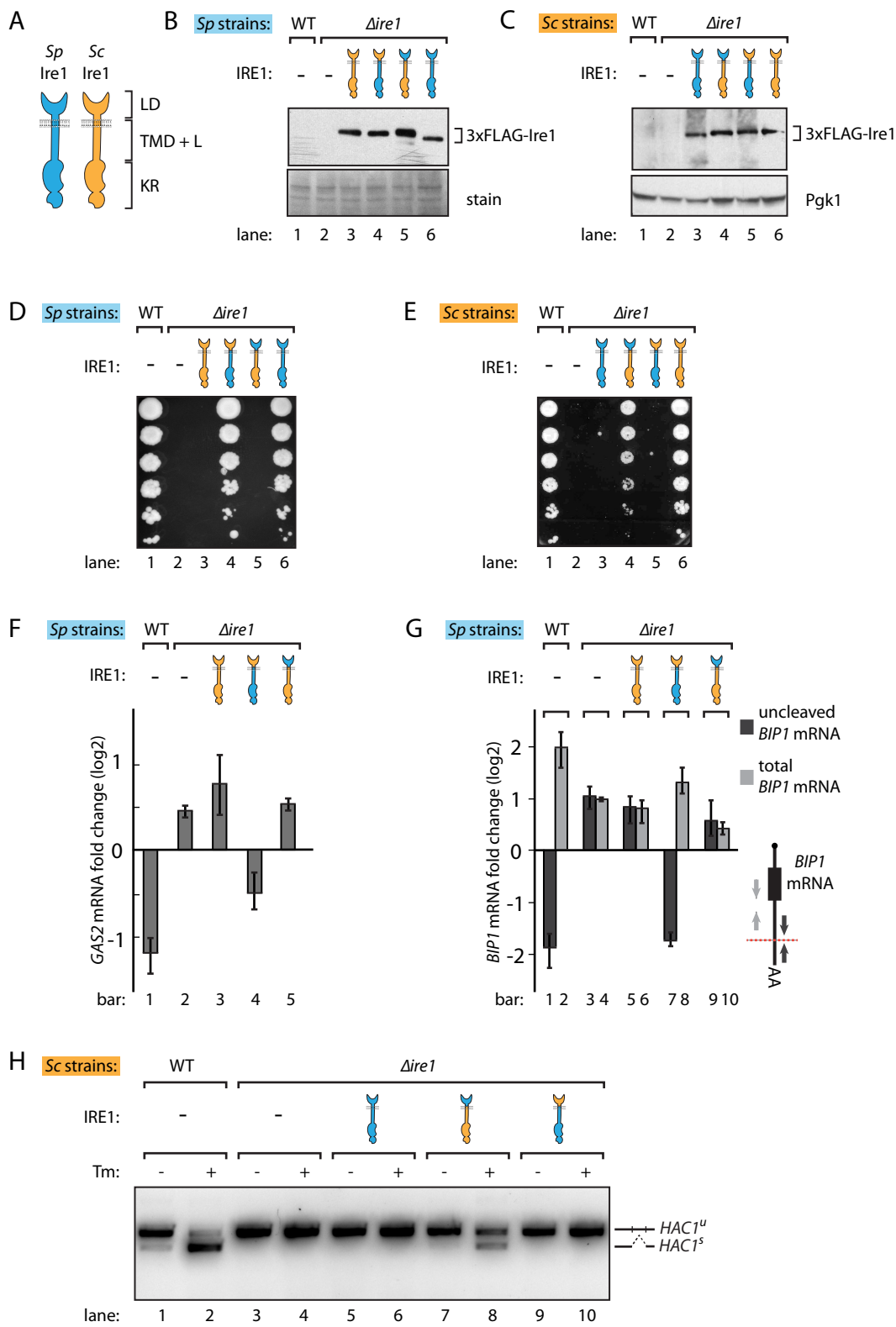


Fig. 1-figure supplement 1 Li et al.

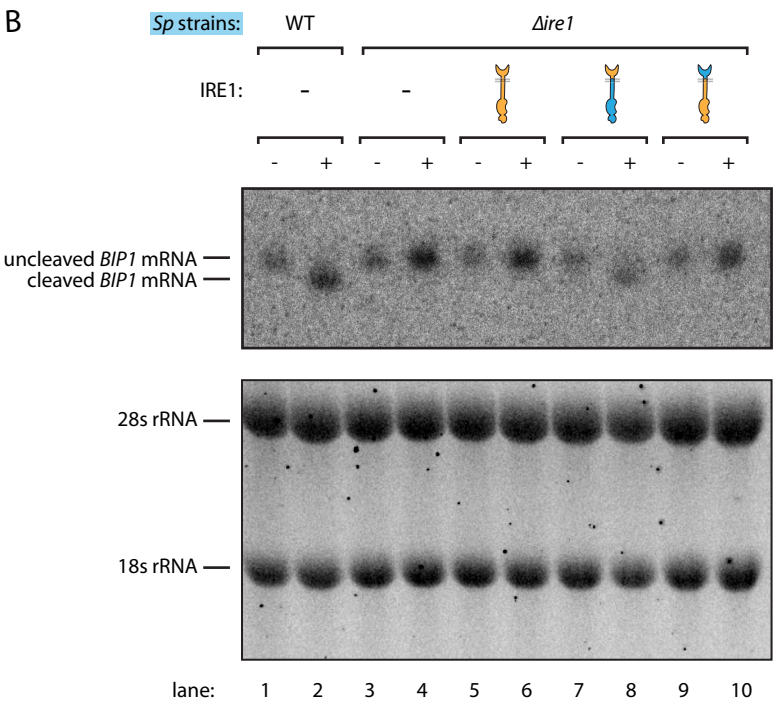
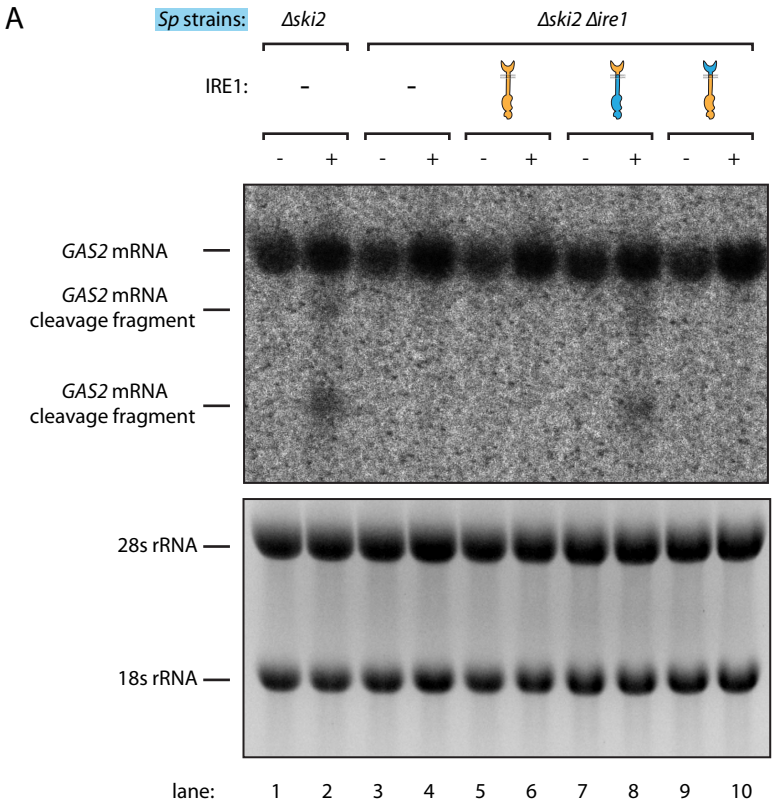
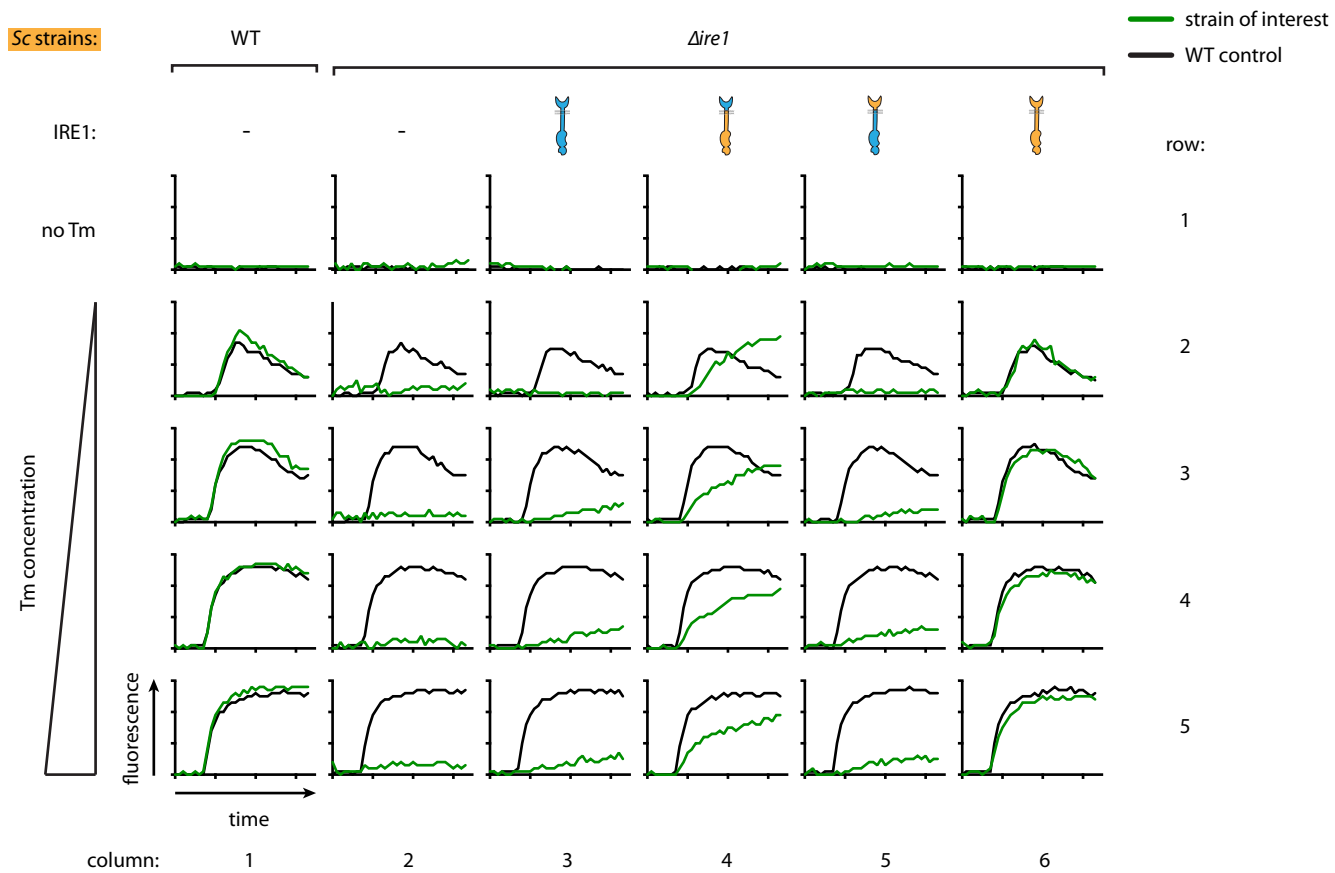


Fig. 1-figure supplement 2 Li et al.

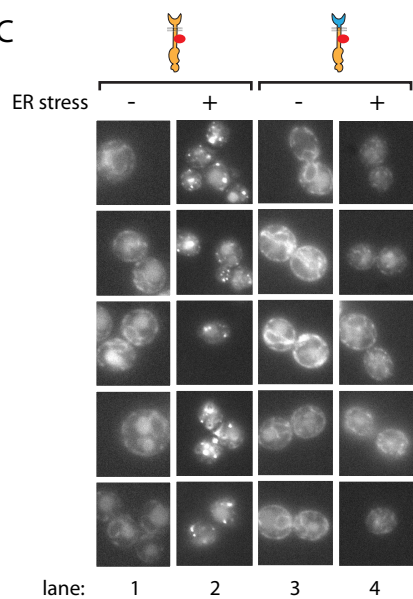
A



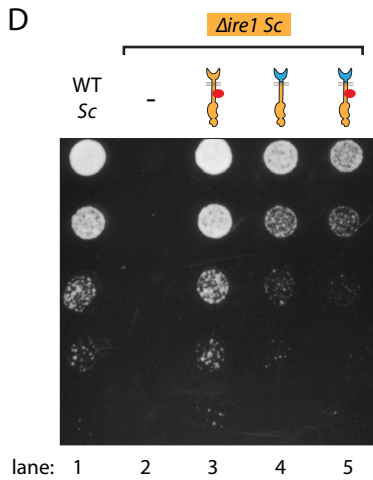
B

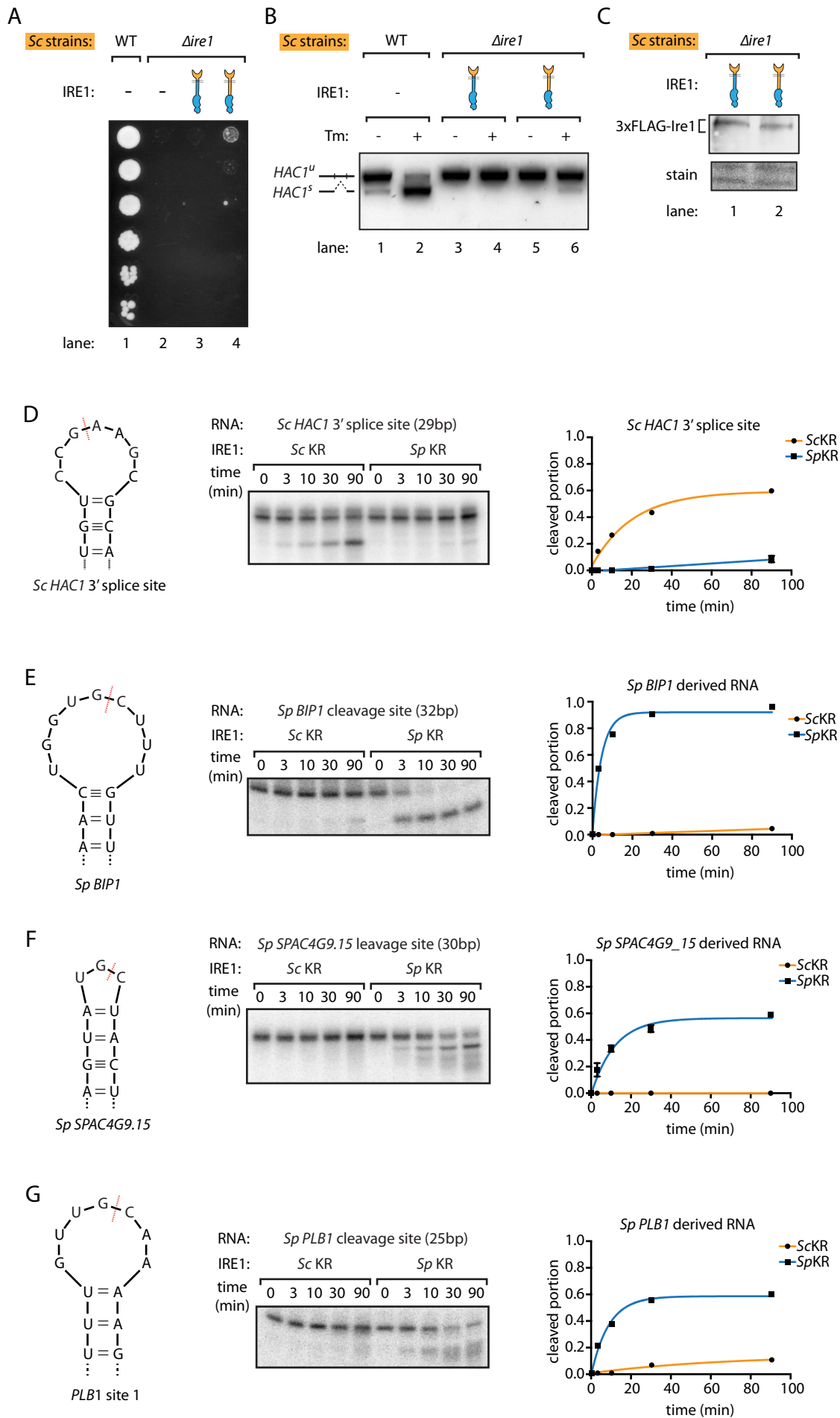


C



D





A

systematic ID	gene name	Ire1 cleavage site sequence
SPBC29A10.08	<i>GAS2</i>	ACGAUCCUGUCGGUU AUGC UGGUGCCGAU AUUC CGU
SPAC22A12.15c	<i>BIP1</i>	AA C ACCUAGUUAACUGG UGC UUUGUUUUCUUUGUAUUG
SPAC26A3.01	<i>SXA1</i>	A UUAUCGGUUUGUC AGU UGC CAUGACU AU UACUGGUAU
SPBC25H2.06c	<i>HRF1</i>	GAGCUAUUUUGGCCUU CGUGC UAGUAAGGCUUGUGCUGU
SPAC1A6.04c	<i>PLB1</i>	UCCUUUGUGGCCUUUGU UGC A AAGGGUCGUGAUGUCG
SPBP4G3.02	<i>PHO1</i>	AUUUGCAGUUAUGAAAU UGC CCUUCA AG ACUAU AG CGA
SPCC970.03		CAUUU A UCGUUUCCGUC UGC CUCGCGCU AA CGAUGUUC
SPBC29A10.08	<i>GAS2</i>	GCUGU CG CUU AC GUUC CGUGC UGCCGUUCGUGAUUCCAA
SPAC1A6.04c	<i>PLB1</i>	GUUGCCGA AAA GGCC AAUGC UGGCCUU ACA UCA AG UCU
SPBP4G3.02	<i>PHO1</i>	A UCUUUGGAGGUGCCUA UGC U A UAGCCUUGCAAUUC
SPBC3D6.02	<i>BUT2</i>	CUU AG UGCUGACAUUCC UGC CAAGUCUAGCCGU C UCUU
SPAC56F8.07		C UUUUACU AC GACAUGG UGC UGCAUGUUCGAGUUUUU
SPCC830.08c	<i>YOP1</i>	GCCUUCUUUAGUAUCA UGC U A UUGA AA CUACUA ACA A
SPAC4G9.15		GG A UCGGUAA AG AGUA UGC UACUCAAUUAGCCAUGUC

B

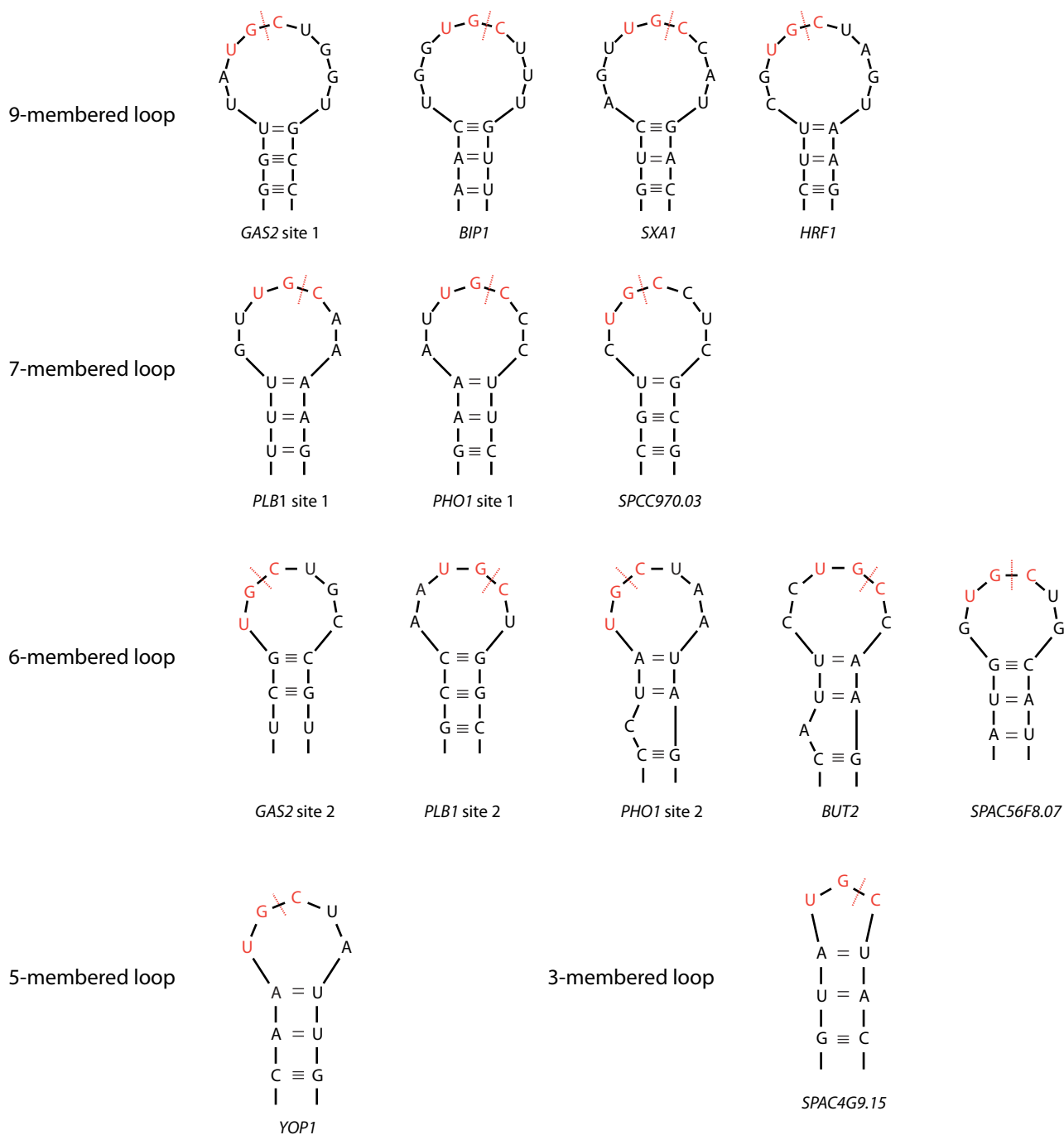


Fig 4 Li et al.

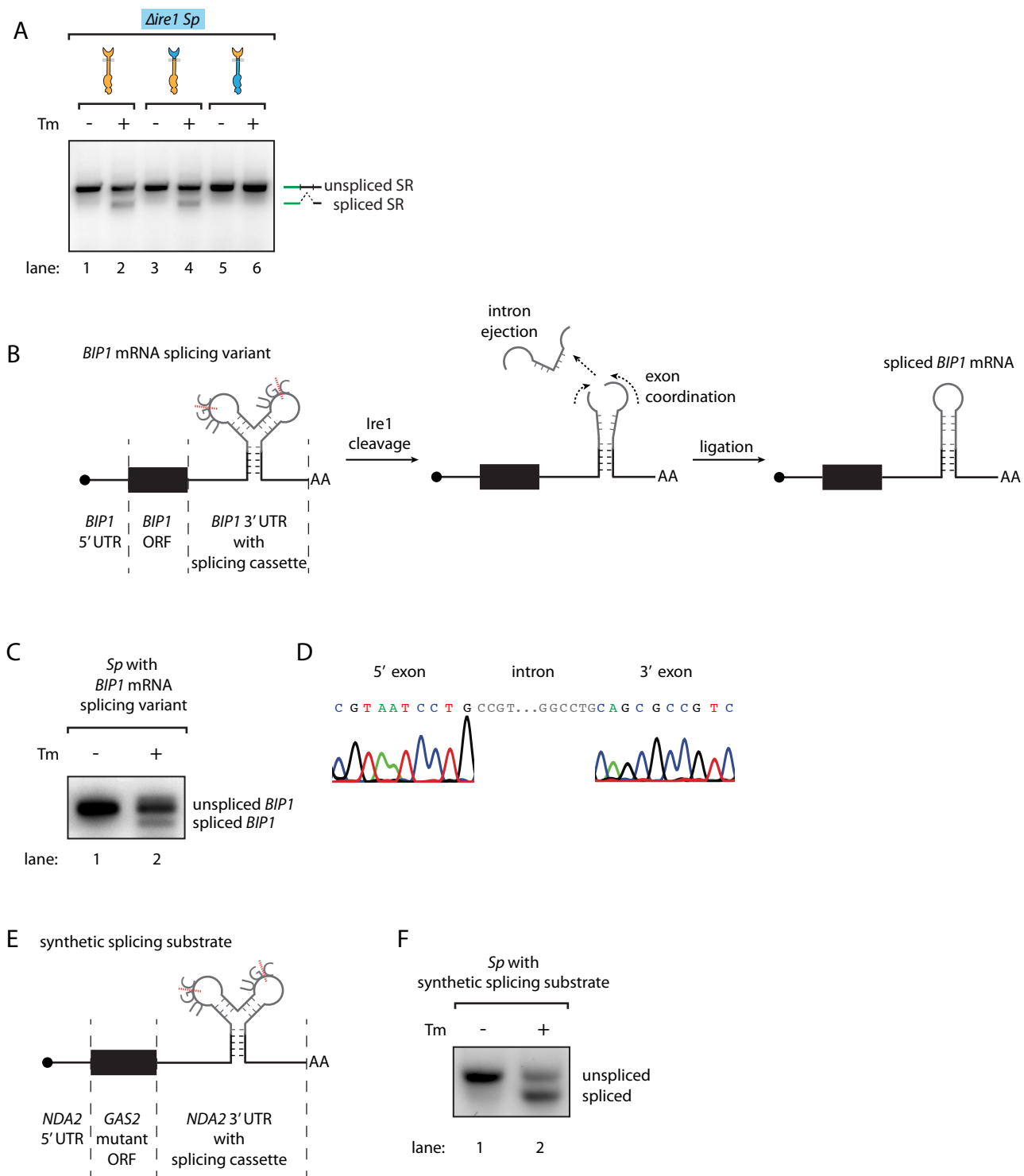


Fig. 4-figure supplement 2 Li et al.

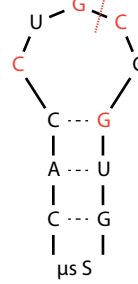
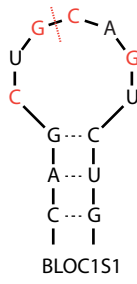
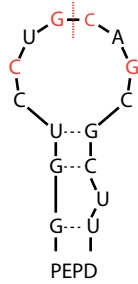
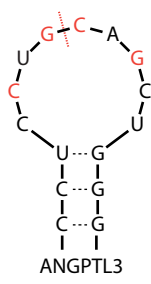
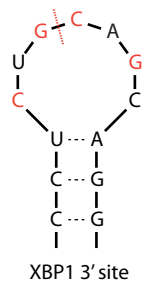
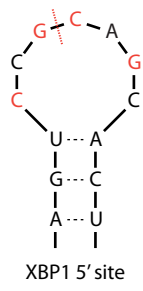


Fig. 4-figure supplement 3 Li et al.

A

```

IRE1alpha  1  LEKQLQFFQDVSDRIEKESLDGPIVKOLERGGRAVVKMDWRENITVPLQTDLRKFRITYKG
IRE1beta   1  RAKQLQFFQDVSDWLEKESSEQEPLVRALEAGGCAVVRDNWHEHISMPLQTDLRKFRSYKG
Sc_IRE1    1  KSKKLEFLLKVS DRLEIENRDPPSALLMKFDAGSDFVIPSGDWTVKFKTFMDNLERYRK
Sp_IRE1    1  YAKKLDLFLIDVSDRFEVEERDPPSPLLQMLENNSKSVIGENWTTCLHSSSLVDNLGKYRKY

IRE1alpha  61  GSVRDLLRAMRNKKHHYRELPAEVRETLSLPPDDFVICYFTSRFPHLLAHTYRAMELCSHE
IRE1beta   61  TSVRDLLRAVRNKKHHYRELPEVVRQALGOVPDGFVOYFTNRFPRLLLHTHRAMRSCASE
Sc_IRE1    61  YHSSKIMDLLRALRNKYHFM DLPEDIAELMGPVDPGFYDYFTKRFPNLLIGVYMIVKEN
Sp_IRE1    61  DGSKIILDILRVLRNKRHHYQDLPE SVRRVLDLDPDGFTSYFVEKFPMLLLHCYHLVKDVL

IRE1alpha  121  RLFQPYYPFHEPPEPQPPVTPDAL
IRE1beta   121  SLFLPYYPDSEARRPCPGATGR
Sc_IRE1    121  LSDDQILREFLYS-----
Sp_IRE1    121  YEESQFKRYLEY-----
    
```

B

